Segmented helical structures formed by ABC star copolymers in nanopores

Meijiao Liu, Weihua Li, and Feng Qiu

Citation: The Journal of Chemical Physics **138**, 104904 (2013); doi: 10.1063/1.4794785
View online: http://dx.doi.org/10.1063/1.4794785
View Table of Contents: http://scitation.aip.org/content/aip/journal/jcp/138/10?ver=pdfcov
Published by the AIP Publishing

Segmented helical structures formed by ABC star copolymers in nanopores

Meijiao Liu, Weihua Li,[a] and Feng Qiu
State Key Laboratory of Molecular Engineering of Polymers, Department of Macromolecular Science, Fudan University, Shanghai 200433, China

(Received 26 December 2012; accepted 24 February 2013; published online 12 March 2013)

Self-assembly of ABC star triblock copolymers confined in cylindrical nanopores is studied using self-consistent mean-field theory. With an ABC terpolymer forming hexagonally-arranged cylinders, segmented into alternative B and C domains, in the bulk, we observe the formation in the nanopore of a segmented single circular and non-circular cylinder, a segmented single-helix, and a segmented double-helix as stable phases, and a metastable stacked-disk phase with fourfold symmetry. The phase sequence from single-cylinder, to single-helix, and then to double-helix, is similar as that in the cylindrically-confined diblock copolymers except for the absence of an equilibrium stacked-disk phase. It is revealed that the arrangement of the three-arm junctions plays a critical role for the structure formation. One of the most interesting features in the helical structures is that there are two periods: the period of the B/C domains in the helix and the helical period. We demonstrate that the period numbers of the B/C domains contained in each helical period can be tuned by varying the pore diameter. In addition, it is predicted that the period number of B/C domains can be any rational in real helical structures whose helical period can be tuned freely. © *2013 American Institute of Physics*. [http://dx.doi.org/10.1063/1.4794785]

I. INTRODUCTION

The self-assembly of block copolymers under confinement in nanopores is of great interest because confinement can cause the block copolymer to self-assemble into nanostructures beyond those formed in bulk samples.[1] Even with the simplest diblock copolymer, which is characterized by the volume fraction of the minority block, f, and the product of χN, where χ is the Flory-Huggins interaction and N is the total degree of polymerization, the introduction of confinement can enrich the structure formation significantly. In recent years, a large number of studies have been dedicated to explore novel structures formed by bulk lamella-forming,[2–16] cylinder-forming,[16–21] and gyroid-forming[22] diblock copolymers under cylindrical confinement by experiments,[2–5,15,17,18,22] computer simulations,[6–12,16] and theoretical calculations.[13,14,19–21] In the case of bulk lamella-forming diblock copolymers, concentric layers parallel to the pore wall prefer to be formed when the pore wall has a strong preferential interaction to either block. The number of such layers is determined by the pore size relative to the bulk lamellar period.[5,9] If the pore wall is neutral, perpendicular lamellae, with layer normal along the pore axis, are formed, which have a similar period as that in the bulk. The self-assembly behavior becomes more complicated if the pore wall has an interaction with an intermediate strength because no complete wetting layer is formed by either block along the perimeter. For example, Li and Wickham[13] observed I- and Y-shaped structures with translational symmetry along the pore axis, and a perforated-concentric layer structure, using a slightly asymmetric diblock copolymer confined in a cylindrical pore with an intermediate surface interaction. Similarly, in the case of bulk cylinder-forming diblock copolymers, a strong preferential surface interaction can reduce the complexity of self-assemblies, and the corresponding phase behaviors have been well understood by both experiments[23] and theories.[19,21] A generic phase sequence, from a single straight cylinder (C_1) phase, to a stacked-disk (DK) phase, to a single-helix (H_1) phase, to a double-helix (H_2) phase, and so on, has been constructed.[19–21]

One of the most attractive features in this system is the formation of helical morphologies by the self-assembly of achiral block copolymers, imposed by the cylindrical confinement. It has been proposed that to curve the cylinder into a helix is an efficient way to reduce the entropy loss due to chain stretching induced by a mismatched large pore size while keeping the size of the cylinder formed by the minority block close to the bulk radius.[19,20] One expects that the formation of helical morphologies is generic in confined block copolymers, including geometrical confinement, and *soft* confinement which is effectively formed by external environments, such as micelles in solution,[24–27] and the self-assembly of a cylindrical domain of B/C blocks in an A matrix, in linear ABC triblock terpolymers.[28–30] Until now, to our best knowledge, all of observed helical structures contain only homogeneous helix which has the screw symmetry. No doubt we can obtain more intriguing helical morphologies by varying the confining boundary or the block copolymer itself. Recently, a few studies have turned to focus on the self-assemblies of ABC triblock terpolymers confined in nanopores.[31–34] In the ABC star triblock terpolymers, one of the most fascinating features is the assembly of the three-arm junctions during the structure formation, which is usually aligned along straight lines as along as the three blocks are long enough to phase separate.[35–37] After a cylindrical confinement imposed, the assembly of the junctions is enforced to be changed.

[a]E-mail: weihuali@fudan.edu.cn.

Xu *et al.*[34] observed both straight alignment of the junctions in a number of metastable two-dimensional (2D) flower-petal patterns and curved alignment of the junctions in the three-dimensional (3D) morphologies with a hierarchical-lamella forming star terpolymer. As we know, a hexagonally-arranged cylinder phase, where each cylinder segments into alternative B and C domains, can become stable instead of the hierarchical lamella in the bulk when the volume fraction of the symmetric B and C blocks is reduced. Intuitively, it is expected to observe inhomogeneous helical morphologies because of the B/C phase separation within the helix when the hierarchical-lamella forming star terpolymer is replaced by a hierarchical-cylinder forming one in the cylindrical confinement. In this paper we will extend our knowledge on the formation of homogeneous helical morphologies to that of inhomogeneous ones by carrying out a study of the self-assembly of a hierarchical-cylinder forming star terpolymer confined in nanopores using the pseudo-spectral method of the self-consistent field theory (SCFT), which has been often used for the complex block copolymer systems.[30] Our study of the formation of inhomogeneous helical morphologies is motivated by the extensive studies of homogeneous helical morphologies formed in the cylindrically-confined diblock copolymers, and thus our results can be directly compared with those results in the reference model system to reveal the similarity or the difference between them. Furthermore, the alignment of the three-arm junctions in the confinement is more frustrated than that in the bulk. Therefore, the self-assembly of a hierarchical-cylinder forming terpolymer confined in narrow pores is an excellent example to study the impact of the junction alignment on the formation of morphologies, specifically, on the generic phase sequence seen in the confined diblock copolymers. In particular, different morphologies have different ability to release the energy penalty induced by the frustration of the junction alignment. For example, in the straight-cylinder or helical morphologies, the junctions can be readily aligned on precisely or roughly parallel rings. However, for the stacked-disk phase, where B/C co-formed oblate domains are stacked along the pore axis when the A blocks are attracted to the wall surface by the surface preferential interaction and to fill the space between the disks, the junction alignment becomes extremely complicated, and thus may result in the formation of many disk-type morphologies with different junction alignments. In general, the different frustration degrees of the junction alignment can change the relative stability of these phases, and thus change the phase sequence. The theoretical results from the current study can be used to gain a further understanding on the impact of the junction alignment upon the complex self-assembly beyond the bulk system.

II. THEORY AND METHOD

We consider an incompressible melt of ABC star triblock terpolymers confined in a cylindrical pore of diameter $2R = D$, where R is the corresponding radius. The ABC terpolymer, with a total degree of polymerization N, has three block lengths as f_AN, f_BN, and f_CN ($f_A + f_B + f_C = 1$), respectively. The immiscibility between the three blocks is characterized by the products of $\chi_{AB}N$, $\chi_{AC}N$, and $\chi_{BC}N$, respectively, where χ_{ij} (i, j = A, B, C) is the corresponding Flory-Huggins interaction parameter. Spacial lengths in our calculations are expressed in units of the radius of gyration, R_g, of the polymer. Within the mean-field approximation to the many-chain Edwards theory,[39,40] at a temperature T, the free energy F for n Gaussian terpolymer chains confined in a cylindrical pore has the form

$$\begin{aligned}\frac{F}{nk_BT} = &-\ln Q + \frac{1}{V}\int_{|\mathbf{r}|\le R} d\mathbf{r}\{\chi_{AB}N\phi_A(\mathbf{r})\phi_B(\mathbf{r})\\ &+\chi_{AC}N\phi_A(\mathbf{r})\phi_C(\mathbf{r}) + \chi_{BC}N\phi_B(\mathbf{r})\phi_C(\mathbf{r})\\ &-w_A(\mathbf{r})\phi_A(\mathbf{r}) - w_B(\mathbf{r})\phi_B(\mathbf{r}) - w_C(\mathbf{r})\phi_C(\mathbf{r})\\ &+H(\mathbf{r})[\phi_A(\mathbf{r}) - \phi_B(\mathbf{r}) - \phi_C(\mathbf{r})]\},\end{aligned} \tag{1}$$

where $\phi_A(\mathbf{r})$, $\phi_B(\mathbf{r})$, and $\phi_C(\mathbf{r})$ are the volume fractions as function of position. The partition function Q is for a single polymer interacting with the mean fields w_A, w_B, and w_C produced by the surrounding chains. In the confined melts, the spatial integration is restricted to the pore volume, taken to be V. The preference of the pore wall is introduced by including a surface field $H(\mathbf{r})$, $H(\mathbf{r})/\chi N = V_0\{\exp[(\sigma + |\mathbf{r}| - R)/\lambda] - 1\}$ for $R - \sigma \le |\mathbf{r}| \le R$, while $H(\mathbf{r}) = 0$ for $|\mathbf{r}| < R - \sigma$. In this work, we choose the cutoff distance for the surface interaction to be $\sigma = 0.5R_g$, and the decay length to be $\lambda = 0.25R_g$. $V_0 = -0.1$ gives a rather strong preference of the pore wall to A block.

Minimization of the free-energy with respect to the volume fractions and the mean fields leads to the following standard mean-field equations[40]

$$w_A(\mathbf{r}) = \chi_{AB}N\phi_B(\mathbf{r}) + \chi_{AC}N\phi_C(\mathbf{r}) + H(\mathbf{r}) + \eta(\mathbf{r}), \tag{2}$$

$$w_B(\mathbf{r}) = \chi_{AB}N\phi_A(\mathbf{r}) + \chi_{BC}N\phi_C(\mathbf{r}) - H(\mathbf{r}) + \eta(\mathbf{r}), \tag{3}$$

$$w_C(\mathbf{r}) = \chi_{AC}N\phi_A(\mathbf{r}) + \chi_{BC}N\phi_B(\mathbf{r}) - H(\mathbf{r}) + \eta(\mathbf{r}), \tag{4}$$

$$\phi_A(\mathbf{r}) = \frac{1}{Q}\int_0^{f_A} ds q_A(\mathbf{r}, s)q_A^\dagger(\mathbf{r}, s), \tag{5}$$

$$\phi_B(\mathbf{r}) = \frac{1}{Q}\int_0^{f_B} ds q_B(\mathbf{r}, s)q_B^\dagger(\mathbf{r}, s), \tag{6}$$

$$\phi_C(\mathbf{r}) = \frac{1}{Q}\int_0^{f_C} ds q_C(\mathbf{r}, s)q_C^\dagger(\mathbf{r}, s), \tag{7}$$

$$Q = \frac{1}{V}\int d\mathbf{r} q_K(\mathbf{r}, s)q_K^\dagger(\mathbf{r}, s), \tag{8}$$

$$\phi_A(\mathbf{r}) + \phi_B(\mathbf{r}) + \phi_C(\mathbf{r}) = 1, \tag{9}$$

where the field function $\eta(\mathbf{r})$ is a Lagrange multiplier used to enforce the incompressibility condition, $\phi_A(\mathbf{r}) + \phi_B(\mathbf{r}) + \phi_C(\mathbf{r}) = 1$. In the above equations, Q is the partition function of single chain in these fields, and $q_K(\mathbf{r}, s)$ and $q_K^\dagger(\mathbf{r}, s)$

($K = A, B, C$) are end-segment distribution functions. The distribution function $q_K(\mathbf{r}, s)$ is proportional to the probability that a polymer chain segment, of contour length s and with one free end, has its other end located at $\mathbf{r}$. These distribution functions satisfy the modified diffusion equations

$$\frac{\partial q_K(\mathbf{r}, s)}{\partial s} = \nabla^2 q_K(\mathbf{r}, s) - w_K(\mathbf{r}, s) q_K(\mathbf{r}, s), \quad (10)$$

$$-\frac{\partial q_K^\dagger(\mathbf{r}, s)}{\partial s} = \nabla^2 q_K^\dagger(\mathbf{r}, s) - w_K(\mathbf{r}, s) q_K^\dagger(\mathbf{r}, s). \quad (11)$$

The initial conditions are $q_K(\mathbf{r}, 0) = q_L^\dagger(\mathbf{r}, 0) q_M^\dagger(\mathbf{r}, 0)$, where $(KLM) \in \{(ABC), (BCA), (CAB)\}$, and $q_K^\dagger(\mathbf{r}, f_K) = 1$. For numerical solution, we employ the pseudo-spectral method of Tzeremes *et al.*[41] and Rasmussen and Kalosakas[42] to solve the modified diffusion equations for the end-segment distribution functions. Similar to our previous work,[19] the cross-section of the pore is put in a rectangular cell which is a little larger than the diameter of the pore. In our calculations, we discretize the cell into $N_x \times N_y \times N_z = 128 \times 128 \times 64$ lattice, and the chain contour is divided into 100 segments. More details of the calculations can be found in our previous work.[19]

III. RESULTS AND DISCUSSION

To form the hexagonally-arranged segmented cylinders, we choose an ABC terpolymer with fixed symmetric volume fraction of $(f_A, f_B, f_C) = (0.78, 0.11, 0.11)$, and fixed interactions of $\chi_{AB}N = \chi_{AC}N = \chi_{BC}N = 60$.[37] Two feature sizes are introduced to characterize the periodicity of the bulk hierarchical-cylinder phase, L_0 and h_0, which measures the nearest-neighbor cylinder-to-cylinder distance and the alternative B/C domain period along the cylinder axis, respectively. And they are determined as $L_0 \approx 4.05R_g$ and $h_0 \approx 1.72R_g$ for this given group of parameters. The pore diameter, D, is varied to examine the structure formation of the ABC terpolymer. Here we focus on the case that the pore surface has a strong preferential interaction to the longest A block. In fact, it is a challengeable task to find complex morphologies without a high symmetry in the SCFT calculations. Usually, the employment of special initial conditions for the mean fields is helpful during the search of new morphologies. For example, a random initial condition but with a screw symmetry can facilitate the localization of the saddle point toward the formation of helical morphology in the cylindrically-confined diblock copolymers even though the helical phase is only metastable. For the formation of segmented helical morphologies here, the situation is more complicated. When the screw symmetry is broken, the helical length cannot be varied continuously, but by an integer period of B/C domains. With the periodic boundary condition, which is commonly used for the direction along the pore axis, we have to set the repeating number n_{BC} of B/C-domains contained in each period of helix, and vary n_{BC} to optimize the free energy. For this purpose, we first generate density configurations of segmented single/double helical morphologies using strong-segregation approximation, where the interfaces are ideal step function, and then use it as the input to produce the initial fields with the field equations (2)–(4) for the SCFT solvation process. Within the simple scheme, various integers of n_{BC} can be set by hand. For the stacked-disk phase, a homogeneous disk-type density configuration with a B/C mixing state is applied as the initial condition, and usually a large number of runs are tried to look for different disk-type morphologies. With these found morphologies, we can sieve our the stable morphologies, and thereby identify a stable phase sequence with respect to the pore diameter by comparing their free energy.

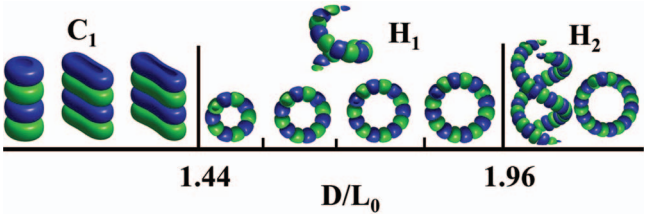

FIG. 1. Phase diagram of morphologies formed by the ABC star terpolymer confined in narrow nanopores with varying pore diameters, D, in units of L_0. The pore wall has a strong attraction to the A component; the A component is not shown in this figure for reasons of clarity. We plot the isosurfaces of B/C volume fractions (indicated by green/blue color) of morphologies, including three different-shape morphologies for the single-cylinder phase, C_1, four single-helix, H_1, morphologies with different repeat numbers of B/C domains in a helical period, and one morphology for the double-helix phase, H_2. The top views of the single-helix and double-helix morphologies indicate that the repeat number of n_{BC} from left to right is 5, 6, 7, 8, and 10, respectively. For the reason of clarity, only one helix is plotted in the top view of the double-helix morphology.

In Figure 1, a phase sequence, together with the B/C-isosurface plots of corresponding morphologies, is presented. By comparing the free energy between all candidate phases, three categories of phases, segmented single circular or non-circular cylinder (C_1), segmented single-helix with various repeating B/C segments in each helical period, and segmented double-helix, are identified to be stable. There are a few notable features in this phase diagram. The first one is that the phase sequence is generically similar as that in the cylindrically-confined diblock copolymer, i.e., from single cylinder, to stacked-disk, to single-helix, and to double-helix. This suggests that the phase separation between B and C blocks does not influence the formation and stability of helical phases dramatically. However, there is also difference, namely, that the stacked-disk phase is absent as a stable phase. A detailed discussion will be given later. The second feature is that the shape of B/C co-formed cylinder in C_1 changes continuously from circular to be elongated along the radial direction as the pore size increases, which is not observed with the homogeneous C_1 in the confined diblock copolymer. In some sense, the elongated cylinder can be seen as the fusion of two circular cylinders enforced by the geometrical confinement. Obviously, this deformation is stabilized by the new factor, i.e., the alignment of three-arm junctions. When the pore size is increased, a large portion of A block has to enter the central part of B/C interface if the circular B/C domain shape is maintained, and thus induces a high A/B and A/C interfacial energy. To elongate the circular B/C interface is an effective way to reduce the distance of A block inside the B/C interface. However, at the same time, it results in an energy penalty because of the highly nonuniform mean curvature of

B/C domains.[38] The nonuniformity of the mean curvature is amplified as the pore size is raised, and thereby it drives the phase to transform into segmented single-helix, H_1. As we mentioned previously, the repeating number of B/C segments in a helical period, n_{BC}, can be tuned during the formation of the single helix. In our theoretical calculations, only integer n_{BC} can be considered because of the implementation of the periodic boundary condition. Of course, n_{BC} is not necessary to be an integer and can be any rational when the helical structure contains a large number of helical periods in real experimental samples. To estimate the average value of n_{BC} per helical period more accurately, we have to consider helical structures with many helical periods, which would raise the burden of calculations. However, the integer n_{BC} is a reasonable approximation for the rational value when there are many repeating B/C domains in one helical period. This approximate value can be used to estimate the other characteristics of helix, including the pitch angle, the average B/C-domain period along the helix, and the helical screw radius. Consequently, the third intriguing feature is that there are a few *artificial* morphologies of H_1 with $n_{BC} = 5$, 6, 7, and 8 in the phase diagram. In addition, the phase transition between H_1 and H_2 occurs at $D \approx 1.96\,L_0$, which is very close to the value, $D \approx 2.04\,L_0$ of Figure 1(a) in Ref. 19. When the single-helix phase transfers to the double-helix phase, the pitch angle or the helical period becomes much larger in order to keep a reasonable length ratio between the helices and the pore. Under the strong-segregation approximation, the sine value of the pitch angle in the double-helix morphology is only half of the single-helix one (see Eq. (12) in Ref. 19). As a consequence, each helix in the double-helix phase has a slightly larger n_{BC} than the single-helix phase at the transition point between H_1 and H_2. It is observed that the double-helix phase of one helical period with the lowest free energy is $n_{BC} = 10$ at $D \approx 1.96\,L_0$.

Different from the cylindrically-confined diblock copolymer, there is no stable stacked-disk phase. In the simple diblock copolymer system, the stacked-disk phase appears as an intermediate phase between C_1 and H_1, and occupies a narrow phase region, where the chain packing is extremely frustrated. Compared with the previous system, the constraint on the arrangement of the three-arm junctions in the present system adds more frustration onto the chain packing. In another word, the phase separation between B and C blocks enrich the formation of stacked-disk type morphologies by varying the arrangement of B and C domains in the disk. In Figure 2(a), we present the free-energy comparisons between those morphologies of C_1, stacked-disk, and H_1. Here the free energy of only one of stacked-disk morphologies is plotted as an example, which is denoted as DK_4 as it has fourfold symmetry. This symmetry makes it have lower free energy than other stacked-disk morphologies with poorer symmetry. The concave property at the central portion of the disk is noticeable. Figure 2(a) suggests that DK_4 becomes more favorable than C_1 when $D \gtrsim 1.44\,L_0$, but has consistent higher free energy than H_1 of $n_{BC} = 5$. Therefore, C_1 directly transfers to H_1 of $n_{BC} = 5$ without DK_4 as an intermediate stable phase. In Figure 2(b), the free-energy comparison between the H_1 morphologies with various n_{BC} shows that there are first-order

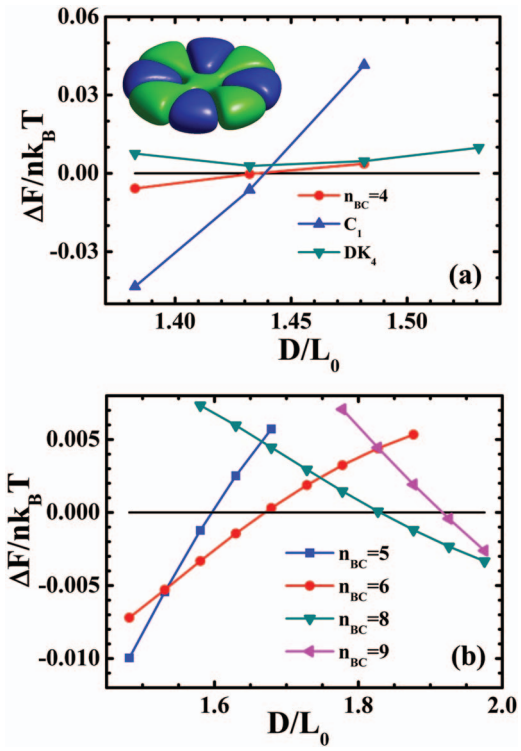

FIG. 2. (a) Free energy of different morphologies relative to that of the single helix with $n_{BC} = 5$, indicated by the horizontal solid line at $\Delta F = 0$. The plot of the volume-fraction isosurface of a fourfold stacked-disk phase, DK_4, is also shown. (b) Free energy of morphologies of the single helix with various n_{BC}. Here the free energy of the helical morphology with $n_{BC} = 7$ is used as a reference.

transitions between these *artificial* morphologies. In order to understand these phase transitions, different contributions of the free energy, the A/B (or A/C) interfacial energy U_{AB} (or equivalent U_{AC} in the B/C symmetric terpolymer), the B/C interfacial energy U_{BC}, and the entropy energy (or stretching energy), $-TS$, are presented in Figure 3. The comparisons reveal that C_1 has the most favorable U_{AB} and U_{BC}, but the most unfavorable entropic contribution. The superiority of C_1 on U_{AB} is because the chain along the radial direction is uniformly stretched while keeping the B/C-domain period constant as the pore diameter increases, and thus the A/B interfacial area per chain becomes smaller and smaller. At the same time, the B/C interface per chain is kept as almost invariant. As a compensate, the stretching energy becomes increasingly high as the pore size increases. Both H_1 and DK_4 are more favorable to reduce the entropy loss due to the high chain stretching than C_1. In large pores, H_1 has less entropy loss than DK_4. In addition, DK_4 is also unfavorable in the B/C interfacial energy relative to H_1 as it has more complex B/C interfaces. On the other side, the arrangement of the three-arm junctions in DK_4 is less preferred than that in H_1, where those junctions are aligned on roughly parallel rings around the helix. Consequently, the H_1 phase is also preferred as it can reduce the entropy loss by regulating the number of B/C domains in the helix as well as the screw radius at a low expense of the interfacial energy. When the B/C domains melt together for low $\chi_{BC}N$, the disadvantage of the DK_4 phase on B/C interfacial

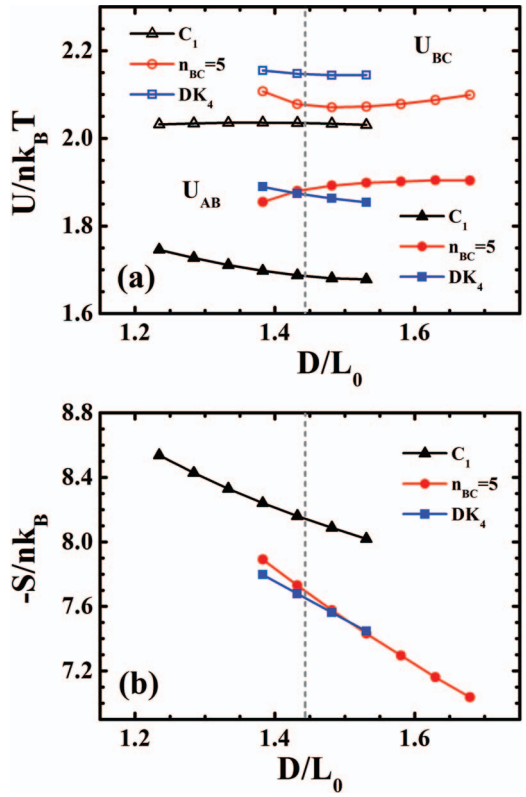

FIG. 3. Comparison between different free-energy contributions for the morphologies C_1, H_1 of $n_{BC} = 5$, and DK_4: (a) interfacial energy contributions of U_{AB} and U_{BC}; (b) entropy, S. The dashed lines indicate the first-order transition between C_1 and H_1.

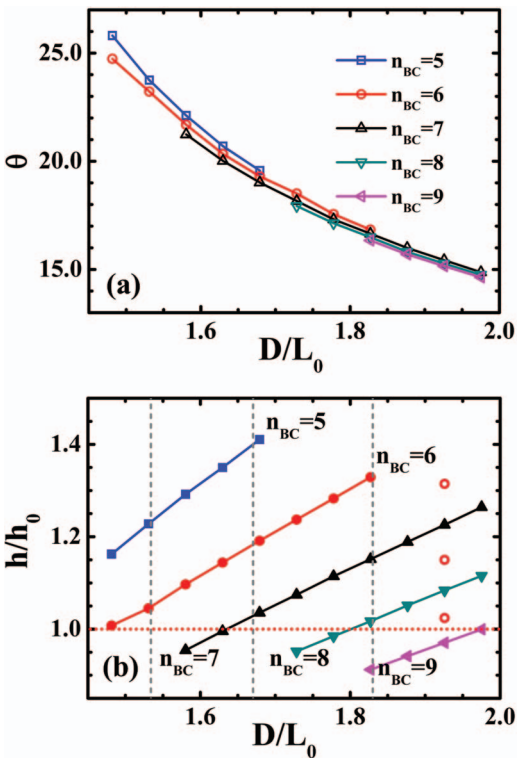

FIG. 5. (a) Pitch angle θ of the single helix for various n_{BC}, as a function of the pore diameter, D. (b) Average B/C-domain thickness, h, along the helix axis, in units of the bulk value of h_0. The three unfilled circles indicate those values of h obtained for $2*n_{BC} = 13$, 15, and 17, from the top down, respectively, in the case of double helical periods. The dashed lines indicate these transition points between the H_1 morphologies with various values of n_{BC}.

energy is reduced, and thus DK_4 will become stable as an intermediate phase between C_1 and H_1.

In Figure 4, we present the free-energy comparisons between H_1 and H_2 for two pore sizes near their transition, $D = 7.8R_g$ (filled symbols) and $D = 8.0R_g$ (unfilled symbols), respectively. Here we examine two helical periods for the two helical phases to show the impact of inaccurate value of n_{BC} on the free energy. We can see that the optimum value of n_{BC} of H_1 is very close to 16, and that of H_2 is close to 19 with $D = 7.8R_g$ in the case of double helical periods. After minimizing the free energy of H_1 and H_2 with respect to the ratio between the helical period and the B/C-domain period, we can see that H_1 has lower free energy than H_2 at $D = 7.8R_g$. When the pore diameter is increased to $8.0R_g$, the stable phase becomes H_2. In addition, the optimum values of n_{BC} of both phases shift toward the increasing direction. This suggests that we have to take a large number of helical periods into account in order to determine the relative stability between segmented helical phases more accurately. Fortunately, the influence of n_{BC} on the free energy, thus on the relative stability between phases, is limited even though we simply use the optimum integer n_{BC} contained in only one helical period as the approximation of its optimum rational. Of course, the choice of integer n_{BC} gives rise to those *artificial* morphologies and their phase transitions for H_1 in Figure 1. In fact, the value of n_{BC} can be varied continuously as the pore size in experiments usually has a large length. We also find that the impact of inaccurate n_{BC} on the pitch angle, $\theta = \arctan(L_p/2\pi R_s)$, where L_p is the helical period and R_s is the helical screw radius, is also small. For example, the difference of the pitch angle of H_1 induced by two neighboring n_{BC} integers is within one degree (see Figure 5(a)). The change of the pitch angle as function of the pore diameter in Figure 5(b) is similar as that of the homogeneous single helix formed in the cylindrically-confined diblock copolymers.[19] The B/C-domain period in the segmented helix, h, is readily calculated by $h = \sqrt{L_p^2 + (2\pi R_s)^2}/n_{BC}$. The data of h for different H_1 morphologies are shown in Figure 5(b). The three unfilled circles indicate the corresponding data of $2n_{BC} = 13$, 15, and

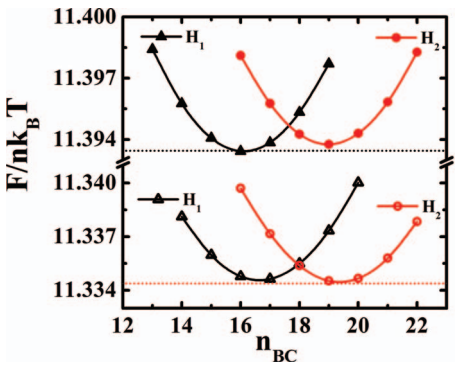

FIG. 4. Free-energy comparisons, at fixed $D = 7.8R_g$ (filled symbols) and $D = 8.0R_g$ (unfilled symbols), between H_1 and H_2. Here, we examine two helical periods of H_1 and H_2. The two dotted lines indicate that H_1 has lower free energy than H_2 at $D = 7.8R_g$, and inversely at $D = 8.0R_g$.

17 in H_1 with double helical periods, respectively. Therefore, the value of h given by them is reasonably intermediate between those of two neighboring integers of n_{BC}. For example, the h value of $2n_{BC} = 13$ is intermediate between those of $n_{BC} = 6$ and $n_{BC} = 7$. This demonstrates how to calculate the helical properties more accurately in the real helical morphologies. The result in Figure 5(b) reveals that the B/C-domain period in H_1 is consistently larger than the bulk value of h_0, and the deviation drops down as the pore diameter increases. This suggests that adding more B/C domains is helpful to release the stretching energy of B/C blocks induced by increased pore size. However, for constant n_{BC}, the B/C-domain period increases as the pore size increasing because the helical length per unit pore length is increased.

IV. CONCLUSIONS

In summary, we have studied the formation of hierarchical morphologies by the ABC triblock terpolymers under the confinement of narrow pores. Specifically we have focused on the ABC star terpolymer, which forms hexagonally-arranged segmented cylinders in the bulk. As the pore size varies, a number of novel morphologies are observed. Though these morphologies resemble the hierarchical feature of the bulk phase, they have their own distinct properties. In very narrow pores, segmented single circular cylinder is formed. Then, as the pore size deviates from the optimum value for single cylinder, the circular cylinder is deformed continuously to be non-circular. And finally, the segmented non-circular cylinder becomes metastable, and is replaced by the segmented single helix. For the segmented helical phase, one of the most attractive features is that its length can be tuned by varying the repeating number of B/C domains along the helix to accommodate the change of pore size. In our SCFT calculations, an integer repeating number of B/C segments in one helical period is considered to be an approximation of the optimum number per helical period in real helical structures with a large length which should contain a large number of helical periods. As a consequence, there are *artificial* phase transitions between the morphologies of the same helical phase, but with various repeating number of B/C segments in one helical period. Our calculations also predict that the ratio between the helical period and the B/C-domain period can be any rational in real segmented helical morphologies. The phase sequence, from single cylinder, to single-helix, and then to double-helix, is similar as that in the cylindrically-confined diblock copolymers except for the absence of the stacked-disk phase. This similarity indicates that the formation and stability of helical structures is generic. The absence of a stable stacked-disk phase in the present system is mainly induced by the phase separation between B and C blocks as well as the constrain of the three-arm junctions. Our results provide a further understanding on the self-assembly of ABC terpolymer systems beyond the bulk one, and might motivate relative experimental research.

ACKNOWLEDGMENTS

This work was supported by the National Natural Science Foundation of China (Grant No. 21174031); the National High Technology Research and Development Program of China (863 Grant No. 2008AA032101). W.H.L. wishes to thank Robert Wickham for helpful discussions and for him to provide the access to the computer resources of SHARCNET (www.sharcnet.ca).

[1] C. R. Stewart-Sloan and E. L. Thomas, Eur. Phys. J. **47**, 630 (2011).
[2] H. Q. Xiang, K. Shin, T. Kim, S. I. Moon, T. J. McCarthy, and T. P. Russell, Macromolecules **37**, 5660 (2004).
[3] K. Shin, H. Q. Xiang, S. I. Moon, T. Kim, T. J. McCarthy, and T. P. Russell, Science **306**, 76 (2004).
[4] H. Q. Xiang, K. Shin, T. Kim, S. I. Moon, T. J. McCarthy, and T. P. Russell, J. Polym. Sci., Part B: Polym. Phys. **43**, 3377 (2005).
[5] M. L. Ma, K. Titievsky, E. L. Thomas, and G. C. Rutledge, Nano Lett. **9**, 1678 (2009).
[6] X. H. He, M. Song, H. J. Liang, and C. Y. Pan, J. Chem. Phys. **114**, 10510 (2001).
[7] P. Chen, X. H. He, and H. J. Liang, J. Chem. Phys. **124**, 104906 (2006).
[8] Q. Wang, J. Chem. Phys. **126**, 024903 (2007).
[9] B. Yu, P. C. Sun, T. H. Chen, Q. H. Jin, D. T. Ding, B. H. Li, and A.-C. Shi, J. Chem. Phys. **127**, 114906 (2007).
[10] G. J. A. Sevink, A. V. Zvelindovsky, J. G. E. M. Fraaije, and H. P. Huinink, J. Chem. Phys. **115**, 8226 (2001).
[11] G. J. A. Sevink and A. V. Zvelindovsky, J. Chem. Phys. **128**, 084901 (2008).
[12] Y. Y. Han, J. Cui, and W. Jiang, Macromolecules **41**, 6239 (2008).
[13] W. H. Li and R. A. Wickham, Macromolecules **42**, 7530 (2009).
[14] S. B. Li, X. H. Wang, L. X. Zhang, H. J. Liang, and P. Chen, Polymer **50**, 5149 (2009).
[15] Y. M. Sun, M. Steinhart, D. Zschech, R. Adhikari, G. H. Michler, and U. Gosele, Macromol. Rapid Commun. **26**, 369 (2005).
[16] J. Feng and E. Ruckenstein, J. Chem. Phys. **125**, 164911 (2006).
[17] Y. Y. Wu, G. S. Cheng, K. Katsov, S. W. Sides, J. F. Wang, J. Tang, G. H. Fredrickson, M. Moskovits, and G. D. Stucky, Nature Mater. **3**, 816 (2004).
[18] H. Q. Xiang, K. Shin, T. Kim, S. I. Moon, T. J. McCarthy, and T. P. Russell, Macromolecules **38**, 1055 (2005).
[19] W. H. Li and R. A. Wickham, Macromolecules **39**, 8492 (2006).
[20] B. Yu, P. C. Sun, T. H. Chen, Q. H. Jin, D. T. Ding, B. H. Li, and A.-C. Shi, Phys. Rev. Lett. **96**, 138306 (2006).
[21] P. Chen, H. J. Liang, and A.-C. Shi, Macromolecules **40**, 7329 (2007).
[22] M. L. Ma, E. L. Thomas, G. C. Rutledge, B. Yu, B. H. Li, Q. H. Jin, D. T. Ding, and A.-C. Shi, Macromolecules **43**, 3061 (2010).
[23] P. Dobriyal, H. Q. Xiang, M. Kazuyuki, J. T. Chen, H. Jinnai, and T. P. Russell, Macromolecules **42**, 9082 (2009).
[24] W. X. Kong, B. H. Li, Q. H. Jin, D. T. Ding, and A.-C. Shi, J. Am. Chem. Soc. **131**, 8503 (2009).
[25] C. I. Huang, C. H. Liao, and T. P. Lodge, Soft Matter **7**, 5638 (2011).
[26] P. Chi, Z. Wang, B. H. Li, and A. C. Shi, Langmuir **27**, 11683 (2011).
[27] L. Q. Wang and J. P. Lin, Soft Matter **7**, 3383 (2011).
[28] U. Breiner, U. Krappe, V. Abetz, and R. Stadler, Macromol. Chem. Phys. **198**, 1051 (1997).
[29] H. Jinnai, T. Kaneko, K. Matsunaga, C. Abetz, and V. Abetz, Soft Matter **5**, 2042 (2009).
[30] W. H. Li, F. Qiu, and A.-C. Shi, Macromolecules **45**, 503 (2012).
[31] J. Feng and E. Ruckenstein, J. Chem. Phys. **126**, 124902 (2007).
[32] P. Chen and H. J. Liang, J. Phys. Chem. B **112**, 1918 (2008).
[33] J. H. Song, T. F. Shi, J. Z. Chen, and L. J. An, J. Phys. Chem. B **114**, 16318 (2010).
[34] Y. C. Xu, W. H. Li, F. Qiu, Y. L. Yang, and A.-C. Shi, J. Phys. Chem. B **113**, 11153 (2009).
[35] T. Gemma, A. Hatano, and T. Dotera, Macromolecules **35**, 3225 (2002).
[36] Y. Matsushita, Macromolecules **40**, 771 (2007).
[37] W. H. Li, Y. C. Xu, G. J. Zhang, F. Qiu, Y. L. Yang, and A.-C. Shi, J. Chem. Phys. **133**, 064904 (2010).
[38] M. W. Matsen, J. Phys.: Condens. Matter **14**, R21 (2002).
[39] A.-C. Shi, *Development in Block Copolymer Science and Technology*, edited by I. W. Hamley (Wiley, New York, 2004).
[40] G. H. Fredrickson, *The Equilibrium Theory of Inhomogeneous Polymers* (Oxford University Press, Oxford, 2006).
[41] G. Tzeremes, K. O. Rasmussen, T. Lookman, and A. Saxena, Phys. Rev. E **65**, 041806 (2002).
[42] K. O. Rasmussen and G. Kalosakas, J. Polym. Sci., Part B: Polym. Phys. **40**, 1777 (2002).